Microfluidic patterning of miniaturized DNA arrays on plastic substrates

Geissler, Matthias; Roy, Emmanuel; Diaz-Quijada, Gerardo A.; Galas, Jean-Christophe; Veres, Teodor

Publisher's version / Version de l'éditeur:
https://doi.org/10.1021/am900285g
ACS Applied Materials and Interfaces, 1, 7, pp. 1387-1395, 2009-07

Article to ACS Applied Materials and Interfaces 2009

Microfluidic Patterning of Miniaturized DNA Arrays on Plastic Substrates

Matthias Geissler,* Emmanuel Roy, Gerardo A. Diaz-Quijada, Jean-Christophe Galas, and Teodor Veres

National Research Council of Canada, Industrial Materials Institute, Boucherville, Québec, J4B 6Y4, Canada

* E-mail: matthias.geissler@cnrc-nrc.gc.ca

ABSTRACT This paper describes the patterning of DNA arrays on plastic surfaces using an elastomeric, two-dimensional (2D) microcapillary system (μCS). Fluidic structures were realized through hot embossing lithography using Versaflex® CL30. Like elastomers based on poly(dimethylsiloxane) (PDMS), this thermoplastic block co-polymer is able to seal a surface in a reversible manner, making it possible to confine DNA probes with a level of control that is unparalleled using standard microspotting techniques. We focus on μCSs that support arrays comprising up to 48 spots each being 45 μm in diameter. Substrates were fabricated from two hard thermoplastic materials – poly(methylmethacrylate) (PMMA) and a polycyclic olefin (e.g., Zeonor® 1060R) – which were both activated with *N*-hydroxysuccinimide (NHS) ester to mediate covalent attachment of DNA molecules. The approach was exemplified by using 0.25 to 32 μM solutions of amino-modified oligonucleotides labeled with either Cy3 or Cy5 fluorescent dye in phosphate buffered saline (PBS), allowing for a direct and sensitive characterization of the printed arrays. Solutions were incubated for durations of 1 to >48 h at 22, 30 and 40 °C to probe the conditions for obtaining uniform spots of high fluorescence intensity. The length (*l*) and depth (*d*) of microfluidic supply channels were both important with respect to depletion as well as evaporation of the solvent. While selective activation of the substrate proved helpful to limit unproductive loss of oligonucleotides along trajectories, incubation of solution in a humid environment was necessary to prevent uncontrolled drying of liquid, keeping the immobilization process intact over extended periods of time. When combined, these strategies effectively promoted the formation of high-quality DNA arrays, making it possible to arrange multiple probes in parallel with a high degree of uniformity. Moreover, we show that resultant arrays are compatible with standard hybridization protocols, which allowed for reliable discrimination of individual strands when exposed to a specific ssDNA target molecule.

KEYWORDS: DNA arrays • plastic substrates • microspotting • fluidic patterning

INTRODUCTION

DNA microarrays (also called DNA chips) (1–3) have become central to a variety of applications that include the mapping, monitoring and sequencing of genes (2, 4), the discovery of novel drugs (5) and, more recently, the diagnostic of infectious diseases (6, 7). DNA microarrays typically comprise a set of pre-synthesized oligonucleotides immobilized on a solid support to be used for competitive hybridization with fluorescently labeled target genes. Thanks to the high specificity of interaction between complementary bases in the strands, a particular hybridization pattern is obtained for each array through fluorescence read-out of the chip using a microarray scanner. As the number of probes in an array determines the amount of information that can be extracted from a single experiment, high-density arrangement is a prerequisite for applications that involve precious and expensive samples or demand for a large number of probes to be screened in parallel.

There are two principal pathways to fabricate DNA chips. One method uses principles of photolithography to synthesize *in-situ* a desired sequence base by base (8). This process can yield arrays of high density (e.g., $>2.5 \times 10^5$ probes per cm^2), but requires sophisticated instrumentation which prevents its wide-spread use in standard microbiology laboratories. In addition, *in-situ* synthesis is limited to relatively short oligonucleotides while high levels of redundancy are necessary since the yield of each synthesis step can vary. Another and generally more accessible way is microspotting, which involves the delivery of minute amounts of a DNA solution either through robotic handling of metal pins (1, 9) or by using drop-on-demand technologies (10, 11). The spot diameter that is obtained with current commercial arraying techniques is typically between 500 and 80 μm depending on the precision of the instrument, the experimental details of the spotting process, and the surface characteristics of the substrate. Although it has been demonstrated that spots ranging from the micrometer scale to below 100 nm can be realized when sufficiently miniaturized pins are employed (12, 13) much interest remains in the development of techniques that allow for routine access to spots of an intermediate size regime. For example, many screening applications in medical diagnostics require only a limited number probes (e.g., less than 100), and spot diameters of 60 to 20 μm would facilitate accommodation of the corresponding arrays in appropriate lab-on-a-chip (LOC) devices (14, 15). In addition, most commercial microarray scanners support signal detection with a lateral resolution of $\gtrsim 5$ μm, making read-out of hybridization events, at present, more reliable for larger than for smaller spots.

Traditionally, glass has been among the most favorable materials for DNA microarrays; it offers high mechanical stability, low intrinsic fluorescence background, and its surface can be modified with a variety of functional groups using silane chemistry (9). On the other hand, glass is relatively expensive and difficult to micromachine, motivating considerable research and development efforts towards plastic-based supports (16–22) for DNA arrays, especially when disposable, low-cost LOC platforms are the fabrication target. A number of hard thermoplastic materials including poly(methylmethacrylate) (PMMA), polycarbonate or cyclic olefin co-polymers seem promising to this end because these materials i) are relatively inexpensive, ii) provide robustness and durability at low specific weight, iii) allow for large-scale replication using well-established techniques based on molding or embossing, and iv) can be bonded (either permanently or reversibly) to other surfaces, which is key to the assembly and packaging of LOC devices. Furthermore, interfacial properties such as wetting, surface charge, compatibility with biological species, or reactivity towards functional groups can be altered conveniently for many polymers to comply with the requirements of a particular application. The use of optical grade materials with low intrinsic fluorescence background constitutes another prerequisite for on-chip fluorescence-based detection of DNA hybridization events (20, 23, 24).

Microfluidics is generally perceived as a means of manipulating minute amounts of liquid using channels (or capillaries) with micrometer dimensions (25–28). Features that make the use of microfluidic systems advantageous are i) low sample consumption, ii) accurate registration and positioning, iii) high parallelism, and iv) good control over reaction conditions, among others. Flow in microchannels is typically characterized by low Reynolds numbers with molecular diffusion being the dominant driving force in supplying reagents under the conditions of laminar flow. Convection can be achieved through the implementation of bas-relief structures (29), split-and-recombine systems (30, 31), or multivortex segments (32). It is equally possible to employ several active methods such as magnetic stirring (33) or acoustic actuation (34). With the advent of soft lithography (35, 36), elastomer-based microcapillary systems (μCSs) became accessible to a broader scientific community, thus effectively promoting their use in surface processing and patterning. Elastomers are advantageous to a number of fluidic applications because these materials i) conform to smooth substrates, ii) provide a watertight seal to the surface, and iii) can be removed from the substrate upon processing, often without leaving notable residues on the surface. The concept of fluidic patterning has been shown for a variety

of materials, most notably biological species such as DNA (16, 37), proteins (38–40) and cells (41, 42) immobilized silicon, glass and plastic supports. At present, most fluidic-based arrays comprise a set of simple and continuous lines arranged in a parallel fashion, although the formation of discontinuous features using multi-level networks has also been demonstrated (42, 43). In addition to patterning, fluidic devices have come into focus as a means of performing amplification (44) or hybridization reactions (45–47) with oligonucleotides in a time- and cost-effective manner.

In this paper, we use microfluidics as means of fabricating DNA microarrays on hard thermoplastic substrates with excellent control over size, density, and registration of spots. The μCS described herein comprises a two-dimensional (2D) network of microchannels, which are straightforward to fabricate by hot embossing using a melt-processable (thermoplastic) elastomer (48). The material is capable of sealing a surface reversibly upon contact, and the embedded microchannels can be filled by capillary action – that is the autonomous movement of liquid in small channels based on hydrodynamic forces (43). Immobilization of DNA molecules is achieved through passive incubation with activated plastic supports, although the design of the μCS would also allow for connecting external pumping systems to induce continuous flow or recirculation of probe liquid. We focus on the parameters affecting DNA attachment, and investigate the conditions for obtaining high-quality microarrays of fluorescently-labeled, amino-modified oligomers on PMMA and Zeonor® substrates. We believe that the work presented in this paper contributes to the development of integrated plastic LOC platforms for high-throughput diagnostics using DNA microarray technology.

RESULTS AND DISCUSSION

The μCSs we used in this study were fabricated by hot embossing using sheets of Versaflex® CL30 – a styrenic block co-polymer – in conjunction with a photolithographically-prepared SU-8 master (49). Versaflex® CL30 belongs to the class of thermoplastic elastomers (TPEs), and consists of hard polystyrene domains in a soft, rubbery matrix of poly(ethylene/butylene) (50). Inspection of the surface using atomic force microscopy (AFM) revealed that domains are about 10 to 30 nm in size and distributed with nearly perfect hexagonal symmetry (data not shown). The size of domains generally depends on processing conditions as well as on the molecular

weight of the constituents, and typically ranges from micro- to nanometer length scales (51, 52). Although few published examples exist on the use of TPEs for soft microfabrication, these polymers are currently finding increased attention in areas that traditionally rely on poly(dimethylsiloxane) (PDMS) (35, 36, 53–55) as the enabling material. For example, Trimbach and co-workers employed styrenic block co-polymers for fabricating micropatterned elastomeric stamps for microcontact printing (μCP) (56). These authors further investigated the use of multiblock co-polymers for producing stamps with a certain degree of hydrophilicity (57). Huskens and co-workers demonstrated μCP using block co-polymer stamps in conjunction with surface modification to transfer polar ink molecules onto a solid support (58). Moreover, Ugaz and co-workers employed tailored TPE gels for the fabrication of microfluidic networks (32, 59–61). Embossing of fluidic structures into CL30 was performed within the high-temperature regime of the elastomer, in which the polymer network softened, allowing material to flow and adapt to the shape of the master pattern. Upon cooling, the material solidified, thereby preserving the shape of imprinted features with high fidelity. The smallest feature size that we replicated in the context of this study was on the order of 5 μm, corresponding to the width of both ridges and trenches in the central part of the μCS (Figure 1A). Like for other elastomers such as PDMS, mechanical stability of microstructures was dependent on aspect ratio (62, 63), allowing variation in depth (*d*) of microchannels to a limited extent. For example, the 5-μm-wide ridges could tolerate aspect ratios of up to 1.5 without notable deformation, yet these structures were prone to collapse when approaching an aspect ratio of 2.0 (64).

The central part of the μCS comprised a 2D array of circular cavities each being 45 μm in diameter (Figure 1A). These features were arranged in rows with a periodicity of 60 μm. Arrays included up to six rows, providing a maximum number of 48 spots. Incoming and outgoing supply channels were ~5 μm in width, but broadened to ~50 μm towards the periphery. The overall configuration of the μCS allows for producing DNA microarrays at relatively high density, while, in principle, being compatible with commercially available scanning technology for read-out. We activated plastic substrates to achieve covalent attachment of amino-modified oligonucleotides using procedures that are described in more detail by Diaz-Quijada and co-workers (20). First, carboxylate groups were generated at the surface. For PMMA substrates, this was realized through base-catalyzed hydrolysis; Zeonor® substrates were exposed to ozone gas. In a second step, carboxylic acid groups were converted into reactive esters through treatment with *N*-

hydroxysuccinimide (NHS) and 1-ethyl-3-(3-dimethylaminopropyl)carbodiimide hydrochloride (EDC) (65). Spotting was performed by placing the μCS channel-side down onto an activated slide, as illustrated in Figure 1B. Like other elastomers, CL30 can seal the surface reversibly, resulting in a full-thermoplastic circuitry of enclosed microchannels. Each channel was filled from a macroscopic access point (inlet) to guide a solution of oligomers along the surface of the plastic substrate to produce a spot. Pristine surfaces of Versaflex® CL30 were largely hydrophobic, which necessitated hydrophilization of channels via oxygen plasma treatment to achieve capillary flow of aqueous DNA solutions, circumventing the need of adding any surfactants (66). Immobilization of DNA molecules takes place through displacement of the NHS ester and the formation of a stable amide bond, as depicted in Figure 1B. Finally, the array is recovered by peeling the μCS away from the surface. We validated the performance of the immobilization process using ssDNA in the form of relatively short oligonucleotides (probes **p1** to **p5**) which were modified with amino-groups, and labeled with either Cy3 (λ_{ex} = 550 nm; λ_{em} = 570 nm) or Cy5 (λ_{ex} = 650 nm; λ_{em} = 670 nm) fluorescent dye at the 3′- and 5′-positions of the strand, respectively (Table 1). The employment of fluorescently tagged oligonucleotides allowed for rapid and sensitive analysis of resultant arrays using fluorescence microscopy.

Figure 2 illustrates the evolution of fluorescence intensity (*I*) as a function of incubation time and temperature for a 32 μM solution of **p1** used in conjunction with a PMMA substrate. As shown by the images in Figure 2A, incubation time was central to achieving DNA attachment at the plastic surface. While incubation for 1 h at 40 °C yielded only faint fluorescence signal, a period of at least 6 h was required to reveal the array in a faithful manner. When immobilization was allowed to proceed for longer durations (e.g., 48 h), spots contrasted well with the bare plastic surface. In this example, fluorescence intensity of spots was about 15 times higher than that of the pristine PMMA substrate. Variation in the diameter of spots was marginal (<5%) as the dimensions of the printed DNA features were defined by the design of the μCS and did not depend on the immobilization conditions or the wetting properties of the substrate. Edge definition of spots was usually excellent: transition zones between modified and non-modified regions were short (e.g., <5 μm) irrespective of temperature and incubation time, suggesting that diffusion of DNA molecules along the surface into unexposed areas was limited for any of these conditions. This finding accounts for efficient sealing of the plastic surface by the elastomeric μCS (67). The images further reveal that fluorescence intensity was uniform among spots in

each array (e.g., with a coefficient of variation (CV) <10%), which however was conditional to microfluidic supply channels being comparable in length (l) (see below).

It is apparent from Figure 2B that the immobilization process was sensitive to temperature. Despite the fact that the density of immobilized probes increased when the temperature was raised from 22 to 30 and 40 °C, saturation of the surface was not achieved, indicating that the overall adsorption process was relatively slow under these experimental conditions. We think that hydrolysis did not reduce notably the overall yield of the immobilization process as the NHS ester on the plastic surface remained active for extended periods of time. This result was confirmed by control experiments where we stored activated slides in a solution of PBS for up to 5 h before they were exposed to a solution of oligonucleotides (data not shown). When NHS ester groups were completely absent from the surface, DNA molecules adsorbed nonspecifically, and were washed off the substrate in subsequent rinsing steps (data not shown). Distribution of probes in the spotted areas was generally uniform as can be concluded from the fact that variations in fluorescence intensity were well below 10%. A slight increase in intensity distribution was observed for shorter periods of incubation, however, corresponding to the formation of incomplete, low-density deposits during the initial phase of the immobilization process. After passing a maximum at ~10 h, uniformity of deposits increased with the time of incubation for each of the inspected temperatures, although best results were obtained when incubation was done at 40 °C.

Figure 3A illustrates the trends in fluorescence intensity when we progressively reduced the concentration of **p2** from 32 to 0.25 μM using microchannels that were 7.2, 4.2 and 1.4 μm deep, respectively. As can be expected, average fluorescence intensities subsequently decreased for spots produced with either device. We found, however, that signals varied depending on d: in this series, spots produced with the 7.2 μm device consistently displayed the highest intensities. This finding is consistent with the fact that a larger amount of DNA molecules can be transported in these channels compared to their shallower counterparts. In addition, surface area-to-volume ratios increased by a factor of 1.3 and 2.7 when reducing d from 7.2 to 4.2 and 1.4 μm, respectively, for which depletion of solution along trajectories became more pronounced. When we printed arrays of **p2** onto PMMA using micropins, spots typically displayed notable variations in both diameter and intensity, mainly as a result of uncontrolled dewetting and drying of solution on the surface (68) (data not shown). The use of μCSs circumvented these obstacles,

and histograms of fluorescence emission mostly showed a narrow range of intensities (e.g., <10%) for individual spots when concentrations of between 32 and 4 μM were used, suggesting homogeneous coverage of the exposed surface (Figure 3B). However, we were not able to obtain any useful arrays for concentrations below 1 μM, for which intensity values were approaching that of background fluorescence, even when used in conjunction with a μCS of d = 7.2 μm. We frequently observed that fluorescence signal was confined to the edges of the fluidic structures (Figure 3C), especially when we allowed solutions with a lower DNA concentration to dry inside the channel system.

Depletion was, in addition to handling solutions with a low concentration of oligomers, a limiting factor to the realization of uniform arrays when microfluidic supply channels showed notable differences in l. We demonstrated this effect by using a μCS providing an incremental increase in l over six columns of spots (Figure 4A). When a solution of **p1** was incubated at ambient conditions, resultant arrays displayed striking differences in I recorded for each column, Figure 4B. Resultant intensity decreased linearly from column 1 to 6 by ~85%, corresponding to an overall loss in intensity of –3.4% mm^{-1}. With respect to the conditions of sample preparation, depletion was not the only origin of this relatively pronounced decay, but rather was accompanied by irregular evaporation of solvent during incubation. We were able to reduce the effect of depletion by confining treatment with NHS instead of activating the entire surface of the plastic substrate. With a substantial portion of the reactive area being eliminated along the pathway, selective activation not only led to increased values of I, but also helped reduce the gap in intensity between columns relative to each other. For example, when NHS ester groups were present only at the last ~7 mm before the projected position of the array, average intensities of spots in column 6 were ~43% in comparison to their counterparts in column 1 (Figure 4C), suggesting a reduction in fluorescence signal of –2.3% mm^{-1}. Although we did not elucidate the interaction of oligonucleotides and CL30, it was possible to reduce nonspecific adsorption to some extent by adding trace amounts of surfactant such as sodium dodecylsulfate (SDS) to the DNA solution before incubation. However, the use of surfactants generally diminished uniformity of resultant spots, and we therefore did not pursue this approach any further.

Evaporation of the solvent affects the overall immobilization process by inducing convection and local changes in concentration. Ultimately, reaction comes to a halt once the channel has dried out. We suppressed evaporation by storing samples in a water-saturated atmosphere during

incubation. When combined with selective activation of the substrate, we were able to reduce variation in fluorescence intensity to at least 21%, as shown in Figure 4D. Here, decay of signal was –0.84% mm^{-1}, which was primarily due to nonspecific adsorption of DNA molecules along trajectories. Increasing the temperature to 40 °C during incubation mainly resulted in higher signals for the entire array irrespective of the particular length of supply channels. Even though we did not achieve perfect equilibration of intensity values, the results obtained in the course of these experiments proved indispensible to successfully immobilize DNA molecules and to maintain certain flexibility in the design of μCSs.

Figure 5 shows an example in which we arranged two probes (e.g., **p1** and **p3**) in an alternating manner. We observed fluorescence emission of the respective dyes only in the spotted regions of the plastic surface (Figures 5A and 5B), indicating that probes remained effectively isolated from each other, and no significant cross-talk occurred during charging and incubation. Average fluorescence intensities were ~90 ± 10 and ~77 ± 5 for **p1** and **p3**, respectively (Figure 5C). It should be noted, however, that fluorescence signals are not directly comparable as intensities were adjusted arbitrarily for each dye during data acquisition. We usually observed few defects in the printed arrays: for a complete set of 48 spots, the number of sites comprising a mixture of probes was ~5% on average, yet we were also able to achieve nearly perfect arrays (Figure 5D) on a routine basis. Proper surfaces of both substrate and μCS were a prerequisite for obtaining arrays with low defect densities, making it necessary to assemble the two components in a filtered (e.g., clean-room) environment. Figure 5D further confirms that the periodicity of spots in both *x*- and *y*-directions varied marginally, accounting for excellent registration of spots with respect to one another. However, we determined that the overall area of the printed array was reduced by ~2% in size compared to that of the original SU-8 master pattern. This finding was mainly due to shrinkage of the thermally-processed elastomer sheet upon release from the mold, which may be reduced by optimizing processing parameters, such as temperature, pressure and embossing time.

Figure 6 summarizes the outcome of a hybridization experiment that involved three different oligonucleotide probes immobilized on a PMMA substrate. We have selected **p1**, **p4**, and **p5**, which all are amino-modified 15mers labeled with Cy3 (Table 1). The sequence of these molecules differed, however, as **p1** and **p4** showed mismatches for two consecutive bases (CA *versus* AC, respectively), while **p5** was exclusively composed of T. Figure 6A displays a test

array comprising sets of two neighboring spots for each probe which are separated by PBS serving as a negative control. Cy3 fluorescence intensities were largely comparable for all probes (see below) while reference spots were indistinguishable from the bare regions of the PMMA substrate. We did not detect any fluorescence intensity above background level when we screened the array for Cy5 emission (Figure 6B). Probes were subjected to hybridization with **t1** – a Cy5-labeled oligonucleotide that had a sequence complementary to **p1** (Table 1). As can be predicted, fluorescence intensity varied when the array was imaged in the Cy5 channel: hybridized spots corresponding to **p1** showed the highest intensity; spots of **p4** were both revealed faithfully but emitted significantly less fluorescence signal (Figure 6C). We did not detect any notable fluorescence for spots of **p5** as well as for the PBS control. Figure 6D directly compares fluorescence intensities of all eight spots before and after hybridization. In the as-printed array, I was almost equal for spots of the same probe (CV < 2%), but varied slightly between the three different sets (CV < 10%). The initial uniformity among probes was largely preserved in the hybridization pattern (CV ~ 3%), which allowed probes to be discriminated in a reliable manner. The difference in Cy5 fluorescence emission between **t1** hybridized to **p1** and **p4** was ~40%, which accounts for a significant reduction in affinity between these chains as induced by a mismatch of two neighboring base pairs.

CONCLUSION

The patterning of DNA arrays benefits from the use of μCSs in a number of ways, which include i) good control over immobilization conditions, ii) limited dependency on the wetting properties of a particular substrate, and iii) excellent alignment and registration capabilities. We believe that the demonstrations presented in this paper are encouraging and offer potential for further development. While we exclusively focused on PMMA and Zeonor® substrates, the process described herein should be applicable to a broad range of other materials without the need of drastically altering experimental protocols. It is possible to extent the current design to arrays supporting a larger number of spots; it is likely, however, that the footprint of the μCS increases as a result, which may be a constraint with respect to shape and size of substrates to be used. Although we have shown that printed DNA microarrays are fully compatible with standard hybridization protocols, limits in detection, especially in conjunction with non-labeled oligonucleotide probes remain to be addressed. In addition, the volume of DNA solution used

for producing a single spot in the array was relatively high (here, ~1 μL), and needs to be reduced significantly for the approach to become economically favorable. Recent experiments indicated that considerable reduction of sample consumption can be realized, for example, by implementing specially-designed inlet ports which facilitate transfer of probe liquid from a metal pin.[48] As demonstrated in this article, CL30 is a suitable material for fabricating 2D μCSs as it provides a watertight seal of plastic surfaces, making it possible to confine a solution of reagents with high spatial control. Although the use of an inexpensive, melt-processable elastomer is an incentive for rapid prototyping of disposable micropatterned devices, it remains to be explored whether CL30 represents an ultimate choice for this purpose. Material properties such as permeability to solvents or the effect of ingredients being present in the polymer were not within the scope of this study and await further investigation. The development of methods to functionalize the surface and tailor interfacial properties in a chemically well defined manner should contribute to the level of success that CL30 might achieve in soft microfabrication.

EXPERIMENTAL SECTION

Fabrication of μCSs. Fluidic structures were imprinted into Versaflex® CL30 (GLS Corp., McHenry, IL) using a mold that was prepared by photolithography using SU-8 (GM1040, Gersteltec, Pully, Switzerland) on a 4 or 6″ silicon wafer (Silicon Quest International, Inc., Santa Clara, CA). For the fabrication of a mold, the wafer was first baked on a hot plate at 160 °C for 15 min; SU-8 resist was applied through spin coating, which was followed by a pre-bake at 65 and 95 °C for 5 and 15 min, respectively, using a temperature ramp of 2 °C min^{-1}. Resist was exposed to UV light with a wavelength of 365 nm (Hg i-line) at 280 μJ cm^{-2} through a quartz/Cr mask (HTA Photomask, San José, CA) using an EVG 6200 mask aligner (EV Group, Schärding, Austria). Post-exposure bake was done using the same conditions as for the pre-bake. Resist features were developed in propylene glycol monomethyl ether acetate (Sigma-Aldrich Corp., St. Louis, MO) for 2 min; the wafer was rinsed with isopropanol (Anachemia, Montréal, QC) and dried with a stream of nitrogen gas. Resultant resist pattern was hard-baked at 130 °C for 2 h. Finally, the master was coated with a thin, anti-adhesive layer formed from 1*H*,1*H*,2*H*,2*H*-perfluorooctyl-trichlorosilane (Aldrich) using deposition from the vapor phase under reduced pressure. CL30 was received in the form of pellets; the material was extruded at 165 °C to yield a film that was 3 mm in

thickness. The film was cut to pieces of appropriate size, which were imprinted with the master using an EVG 520 embossing tool (EV Group) operated at 170 °C, an applied force of 2×10^3 N over the entire area of the wafer, and a pressure of 1×10^{-3} mbar. Upon cooling to room temperature, the micropatterned elastomer piece was peeled off the master and cut to its final size. Inlets were typically punched through the material; occasionally channels were opened by cutting off their periphery. Prior to use, fluidic devices were exposed to oxygen plasma (Plasmalab80Plus from Oxford Instruments, Bristol, UK) for 4 min at 100 W, a flux of 20 sccm, and a pressure of 50 mTorr. All fabrication steps were carried out in a clean room environment (class 1000).

Preparation of Substrates. Plastic substrates were prepared from either PMMA (Plexiglas® VS UVT, Altuglas International, Philadelphia, PA) or Zeonor® 1060R (Zeon Chemicals, Louisville, KY). PMMA slides of standard size (25×75 mm^2 in area, 1 mm in thickness) were fabricated by injection molding using a Boy 30A injection tool (Dr. Boy GmbH, Neustadt-Fernthal, Germany) operated at a temperature of 220 to 240 °C, an injection speed of 30 mm s^{-1}, and a pressure of 132 bar. The mold (stainless steel, custom-fabricated) was cooled for 15 s before the slide was released. Zeonor® disks (6″ in diameter) were molded using an Engel 150 injection apparatus (Engel, Schwertberg, Austria) operated at temperatures of between 127 and 134 °C, an injection speed of 45 to 103 mm s^{-1}, and a pressure of 25 bar. Plastic substrates were incubated with methanol (Fisher Scientific, Ottawa, ON) for ~20 min before surface modification. PMMA slides were incubated with a saturated aqueous solution of sodium hydroxide (Sigma-Aldrich) for ~2 h, including 1 h of ultra-sonication. Each slide was thoroughly rinsed with deionized (DI) water (18.2 MΩ cm, Millipore, Billerica, MA), and dried with a stream of nitrogen gas. Zeonor® substrates were subjected to ozone treatment for ~20 min. The set-up consisted of an Ozo 2vtt ozone generator (OzoMax, Inc., Shefford, QC) connected to a home-built glass chamber (~20 cm in diameter); samples were placed on a rotary holder stage inside the chamber to ensure uniform treatment. Substrates were then incubated with a freshly prepared solution of 2 mg (17 μmol) of NHS (Sigma-Aldrich) and 8 mg (42 μmol) of EDC (Sigma-Aldrich) in 100 μL of phosphate buffered saline (PBS, pH 7.4, Sigma-Aldrich). We applied ~3 μL of solution per cm^{-2} of surface area; the solution was spread over the substrate via contact with a glass microscope slide, and the sample was stored in a glass or polystyrene Petri dish (Sigma-Aldrich) at room temperature for ~90 min. Upon removal of the cover slide, the PMMA sample was rinsed with DI water, and dried with a stream of nitrogen gas.

Formation of DNA Arrays. Oligonucleotides were purchased from Integrated DNA Technologies, Inc. (Coralville, IA), and used without further purification. Solutions with concentrations ranging from 32 to 0.25 μM in PBS were used for spotting experiments. The TPE-based μCS was placed channel-side down onto the surface of a freshly activated substrate; contact between the two formed instantaneously, and typically propagated across the entire surface without the need of applying any additional force. Charging was done by placing ~1 μL of DNA solution at each channel inlet using a micropipette. During incubation, samples were kept in a Petri dish or glass container of appropriate size covered with an aluminum foil in order to prevent photo-induced bleaching of fluorescence dyes. Incubation was done at 22, 30 or 40 °C for various durations (see text for details). The humidity chamber used in this study comprised a water containing beaker which was sealed with Parafilm® against evaporation. Upon incubation, the μCS was removed from the substrate; the sample was rinsed with a 0.1% solution of SDS (Sigma-Aldrich) in PBS and DI water to remove non-immobilized oligomers from the surface, and finally dried with stream of nitrogen gas. Each microfluidic device was used only once to prevent interferences with previous experiments. Pin-spotting was performed with a VersArray Chipwriter Pro from Bio-Rad (Hercules, CA) at room temperature and 55% humidity using a single SMP3 microspotting pin from ArrayIt Microarray Technology (Sunnyvale, CA). The sample remained untouched for ~90 min. The slide was rinsed with a 0.1% solution of SDS in PBS and with DI water, followed by drying with a stream of nitrogen gas.

Hybridization. Samples were subjected to hybridization without any prior deactivation step. Arrays were incubated with 25 μL of a 10 μM solution of **t1** in PBS; the solution was spread over the surface through contact with a microscope glass cover slide, and the sample was stored at room temperature in a light-protective container for 3 h. Upon removal of the cover slip, the substrate was first carefully rinsed with a 0.1% solution of SDS in PBS, then with water, and finally dried with a stream of nitrogen gas.

Instrumentation. Angles of contact were measured with a contact angle goniometer (Model 200-F1) from Ramé-Hart Instrument Co. (Netcong, NJ) using DI water as the probe liquid. Images of advancing and receding drops were recorded with a CCD camera and analyzed using DROPimage Standard software. Roughness measurements on plastic surfaces were done using a multi-mode Nanoscope IV atomic force microscope (Veeco Metrology Group, Santa Barbara, CA), operated at ambient conditions and in contact mode using silicon nitride cantilevers (NP-

S20, Veeco) with a spring constant of 0.58 N m^{-1}. For each sample, an area of 3 × 3 μm^2 was imaged at a rate of ~1.0 Hz, and a pixel resolution of 512 × 512. Fluorescence imaging of DNA arrays was performed using an Eclipse TE2000-U inverted fluorescence microscope from Nikon (Melville, NY) equipped with an EM-CCD camera from Hamamatsu (Bridgewater, NJ). For each series of samples, identical settings of data acquisition were used to allow for comparison of detected fluorescence signals. It should be noted, however, that the conditions of imaging varied between different sets of samples. Fluorescence intensities were quantified using ImageJ, a Java-based processing and analysis software (downloaded at http://rsb.info.nih.gov/ij/download.html). Optical micrographs were taken using a Nikon Eclipse L150 optical microscope equipped with a QICAM Fast digital camera from QImaging Corp. (Burnaby, BC).

Acknowledgment. This work was supported in part by Genome Canada and Génome Québec. We thank Régis Peytavi (Université Laval) and André Nantel (BRI/CNRC) for useful discussion, and our colleagues Kien-Mun Lau, Jimmy Chrétien, Michel Carmel, Yves Simard, Hélène Roberge, François Normandin, and Sylvie Bérardi (BRI/CNRC) for technical assistance. We are grateful to Michel G. Bergeron (Université Laval) and Michel M. Dumoulin (IMI/CNRC) for their support.

REFERENCES AND NOTES

(1) *Microarray Biochip Technology*; Schena, M., Ed.; Eaton Publishing: Natick MA, 2000.

(2) Review: Lockhart, D. J.; Winzeler, E. A. *Nature* **2000**, *405*, 827–836.

(3) Review: Heller, M. J. *Annu. Rev. Biomed. Eng.* **2002**, *4*, 129–153.

(4) Higgins, J. P. T.; Shinghal, R.; Gill, H.; Reese, J. H.; Terris, M.; Cohen, R. J.; Fero, M.; Pollack, J. R.; van de Rijn, M.; Brooks, J. D. *Am. J. Pathol.* **2003**, *162*, 925–932.

(5) Review: Debouck, C.; Goodfellow, P. N. *Nat. Genet.* **1999**, *21*, 48–50.

(6) Peytavi, R.; Raymond, F. R.; Gagné, D.; Picard, F. J.; Jia, G.; Zoval, J.; Madou, M.; Boissinot, K.; Boissinot, M.; Bissonnette, L.; Ouellette, M.; Bergeron, M. G. *Clin. Chem.* **2005**, *51*, 1836–1844.

(7) Dawson, E. D.; Moore, C. L.; Smagala, J. A.; Dankbar, D. M.; Mehlmann, M.; Townsend, M. B.; Smith, C. B.; Cox, N. J.; Kuchta, R. D.; Rowlen, K. L. *Anal. Chem.* **2006**, *78*, 7610–7615.

(8) Lipschutz, R. J.; Fodor, S. P. A.; Gingeras, T. R.; Lockhart, D. J. *Nat. Genet.* **1999**, *21*, 20–24.

(9) Review: Pirrung, M. C. *Angew. Chem. Int. Ed.* **2002**, *41*, 1276–1289.

(10) Okamoto, T.; Suzuki, T.; Yamamoto, N. *Nat. Biotechnol.* **2000**, *18*, 438–441.

(11) Gutmann, O.; Kuehlewein, R.; Reinbold, S.; Niekrawietz, R.; Steinert, C. P.; de Heij, B.; Zengerle, R.; Daub, M. *Biomed. Microdevices* **2004**, *6*, 131–137.

(12) Xu, J.; Lynch, M.; Huff, J. L.; Mosher, C.; Vengasandra, S.; Ding, G.; Henderson, E. *Biomed. Microdevices* **2004**, *6*, 117–123.

(13) Demers, L. M.; Ginger, D. S.; Park, S.-J.; Li, Z.; Chung, S.-W.; Mirkin, C. A. *Science* **2002**, *296*, 1836–1838.

(14) *Lab on a Chip*, a series of insight review articles in *Nature* **2006**, *442*, 367–418.

(15) Review: Madou, M.; Zoval, J.; Jia, G.; Kido, H.; Kim, J.; Kim, N. *Annu. Rev. Biomed. Eng.* **2006**, *8*, 601–628.

(16) Li, Y.; Wang, Z.; Ou, L. M. L.; Yu, H.-Z. *Anal. Chem.* **2007**, *79*, 426–433.

(17) Fixe, F.; Dufva, M.; Tellemann, P.; Christensen, C. B. V. *Nucleic Acids Res.* **2004**, *32*, e9/1–e9/8.

(18) Bi, H.; Meng, S.; Li, Y.; Guo, K.; Chen, Y.; Kong, J.; Yang, P.; Zhong, W.; Liu, B. *Lab Chip* **2006**, *6*, 769–775.

(19) Lin, R.; Burns, M. A. *J. Micromech. Microeng.* **2005**, *15*, 2156–2162.

(20) Diaz-Quijada, G. A.; Peytavi, R.; Nantel, A.; Roy, E.; Bergeron, M. G.; Dumoulin, M. M.; Veres, T. *Lab Chip* **2007**, *7*, 856–862.

(21) Liu, Y.; Rauch, C. B. *Anal. Biochem.* **2003**, *317*, 76–84.

(22) Situma, C.; Wang, Y.; Hupert, M.; Barany, F.; McCarley, R. L.; Soper, S. A. *Anal. Biochem.* **2005**, *340*, 123–135.

(23) Noerholm, M.; Bruus, H.; Jakobsen, M. H.; Telleman, P.; Ramsing, N. B. *Lab Chip* **2004**, *4*, 28–37.

(24) Hawkins, K. R.; Yager, P. *Lab Chip* **2003**, *3*, 248–252.

(25) Stone, H. A.; Stroock, A. D.; Ajdari, A. *Annu. Rev. Fluid. Mech.*, **2004**, *36*, 381–411.

(26) *Materials for Micro- and Nanofluidics*, a special issue of *MRS Bull.* **2006**, *31*, 87–124.

(27) Review: Squires, T. M.; Quake, S. R. *Rev. Mod. Phys.* **2005**, *77*, 977–1026.

(28) Review: Delamarche, E.; Juncker, D.; Schmid, H. *Adv. Mater.* **2005**, *17*, 2911–2933.

(29) Stroock, A. D.; Dertinger, S. K. W.; Ajdari, A.; Mezić, I.; Stone, H.; Whitesides, G. M. *Science* **2002**, *295*, 647–651.

(30) Dertinger, S. K. W.; Chiu, D. T.; Jeon, N. L.; Whitesides, G. M. *Anal. Chem.* **2001**, *73*, 1240–1246.

(31) Jeon, N. L.; Dertinger, S. K. W.; Chiu, D. T.; Choi, I. S.; Stroock, A. D.; Whitesides, G. M. *Langmuir* **2000**, *16*, 8311–8316.

(32) Sudarsan, A. P.; Ugaz, V. M. *Proc. Natl. Acad. Sci. USA* **2006**, *103*, 7228–7233.

(33) Lu, L.-H.; Ryu, K. S.; Liu, C. *J. Microelectromech. Syst.* **2002**, *11*, 462–469.

(34) Liu, R. H.; Yang, J.; Pindera, M. Z.; Athavale, M.; Grodzinski, P. *Lab Chip* **2002**, *2*, 151–157.

(35) Review: Xia, Y.; Whitesides, G. M. *Angew. Chem. Int. Ed. Engl.* **1998**, *37*, 551–575.

(36) Review: Michel, B.; Bernard, A.; Bietsch, A.; Delamarche, E.; Geissler, M.; Juncker, D.; Kind, H.; Renault, J.-P.; Rothuizen, H.; Schmid, H.; Schmidt-Winkel, P.; Stutz, R.; Wolf, H. *IBM J. Res. Dev.* **2001**, *45*, 697–719.

(37) Chen, H.; Wang, L.; Li, P. C. H. *Lab Chip* **2008**, *8*, 826–829.

(38) Delamarche, E.; Bernard, A.; Schmid, H.; Michel, B.; Biebuyck, H. A. *Science* **1997**, *276*, 779–781.

(39) Delamarche, E.; Bernard, A.; Schmid, H.; Bietsch, A.; Michel, B.; Biebuyck, H. *J. Am. Chem. Soc.* **1998**, *120*, 500–508.

(40) Bernard, A.; Michel, B.; Delamarche, E. *Anal. Chem.* **2001**, *73*, 8–12.

(41) Takayama, S.; McDonald, J. C.; Ostuni, E.; Liang, M. N.; Kenis, P. J. A.; Ismagilov, R. F.; Whitesides, G. M. *Proc. Natl. Acad. Sci. USA* **1999**, *96*, 5545–5548.

(42) Chiu, D. T.; Jeon, N. L.; Huang, S.; Kane, R. S.; Wargo, C. J.; Choi, I. S.; Ingber, D. E.; Whitesides, G. M. *Proc. Natl. Acad. Sci. USA* **2000**, *97*, 2408–2413.

(43) Juncker, D.; Schmid, H.; Drechsler, U.; Wolf, H.; Wolf, M.; Michel, B.; de Rooij, N.; Delamarche, E. *Anal. Chem.* **2002**, *74*, 6139–6144.

(44) Review: Zhang, C.; Xu, J.; Ma, W.; Zheng, W. *Biotechnol. Adv.* **2006**, *24*, 243–284.

(45) Lee, H. H.; Smoot, J.; McMurray, Z.; Stahl, D. A.; Yager, P. *Lab Chip* **2006**, *6*, 1163–1170.

(46) Benn, J. A.; Hu, J.; Hogan, B. J.; Fry, R. C.; Samson, L. D.; Thorsen, T. *Anal. Biochem.* **2006**, *348*, 284–293.

(47) Lee, H. J.; Goodrich, T. T.; Corn, R. M. *Anal. Chem.* **2001**, *73*, 5525–5531.

(48) Roy, E.; Geissler, M.; Galas, J.-C.; Diaz-Quijada, G. A.; Veres, T. *Lab Chip* **2009**, submitted.

(49) SU-8 is an epoxy-based bis-phenol A novolac resin which is widely used for microfabrication purposes. For example, see: Shaw, J. M.; Gelorme, J. D.; LaBianca, N. C.; Conley, W. E.; Holmes, S. J. *IBM J. Res. Dev.* **1997**, *41*, 81–94. The process conditions for obtaining high-quality patterns with this resist are relatively well established. In addition, SU-8 is stable over a wide range of temperatures and mechanically more robust than many other resist formulations, which enabled us reusing the same master for several embossing cycles without notable degradation.

(50) *Handbook of Thermoplastic Elastomers*; 2nd ed.; Walker, B. M.; Rader, C. P., Eds.; Van Nostrand Reinhold Company, Inc: New York, NY, 1988.

(51) Review: Fredrickson, G. H.; Bates, F. S. *Annu. Rev. Mater. Sci.* **1996**, *26*, 501–550.

(52) Motomatsu, M.; Mizutani, W.; Tokumoto, H. *Polymer* **1997**, *38*, 1779–1785.

(53) Review: Quake, S. R.; Scherer, A. *Science* **2002**, *290*, 1536–1540.

(54) Review: McDonald, J. C.; Whitesides, G. M. *Acc. Chem. Res.* **2002**, *35*, 491–499.

(55) Geissler, M.; Kind, H.; Schmidt-Winkel, P.; Michel, B.; Delamarche, E. *Langmuir* **2003**, *19*, 6283–6296.

(56) Trimbach, D.; Feldman, K.; Spencer, N. D.; Broer, D. J.; Bastiaansen, C. W. M. *Langmuir* **2003**, *19*, 10957–10961.

(57) Trimbach, D. C.; Al-Hussein, M.; de Jeu, W. H.; Decré, M.; Broer, D. J.; Bastiaansen, C. W. M. *Langmuir* **2004**, *20*, 4738–4742.

(58) Sadhu, V. B.; Perl, A.; Péter, M.; Rozkiewicz, D. I.; Engbers, G.; Ravoo, B. J.; Reinhoudt, D. N.; Huskens, J. *Langmuir* **2007**, *23*, 6850–6855.

(59) Sudarsan, A. P.; Ugaz, V. M. *Anal. Chem.* **2004**, *76*, 3229–3235.

(60) Sudarsan, A., P.; Wang, J.; Ugaz, V. M. *Anal. Chem.* **2005**, *77*, 5167–5173.

(61) Sudarsan, A. P.; Ugaz, V. M. *Lab Chip* **2006**, *6*, 74–82.

(62) Delamarche, E.; Schmid, H.; Michel, B.; Biebuyck, H. *Adv. Mater.* **1997**, *9*, 741–746.

(63) Bietsch, A.; Michel, B. *J. Appl. Phys.* **2000**, *88*, 4310–4318.

(64) Versaflex® CL30 has a surface hardness of 30 (Shore A), a tensile strength of 6619 kPa, and an elongation at break of 780% according to the specifications of the supplier. Accessed at http://www.glscorp.com.

(65) NHS esters are reactive towards nucleophilic groups, and are frequently used for the immobilization of biochemical species containing amino-functionalities. For example, see: Johnsson, B.; Löfås, S.; Lindquist, G. *Anal. Biochem.* **1991**, *198*, 268–277.

(66) Extruded pieces of CL30 that were used for device fabrication exhibited advancing and receding contact angles of 108 ± 1° and 84 ± 1°, respectively. Exposure to oxygen plasma rendered the surface somewhat more hydrophilic. After rinsing any possible residues off the surface, we obtained advancing and receding contact angles of 65 ± 2° and 21 ± 4°, respectively, which was sufficient to promote autonomous movement of aqueous solution in the channels. The time required for filling the entire μCS is dependent on *l*, and was typically on the order of 5 to 15 minutes. Oxidized surfaces of CL30 were sufficiently stable in air to ensure convenient handling, yet they largely recovered their hydrophobic character over the course of several days when stored at ambient conditions.

(67) AFM measurements of activated plastic surfaces revealed RMS roughness values that were generally in the lower nanometer range for both PMMA and Zeonor® substrates. The μCS conformed spontaneously to either of these surfaces without the need of applying any external pressure. Forces of adhesion between CL30 and Zeonor® were generally superior

to those of CL30 and PMMA (data not shown), indicating notable differences in the polymer-polymer interactions at the interface.

(68) Deegan, R. D.; Bakajin, O.; Dupont, T. F.; Huber, G.; Nagel, S. R.; Witten, T. A. *Nature* **1997**, *389*, 827–829.

Table 1. Sequences and Modifications of Oligonucleotides Used in this Study

code	sequence	5′ end	3′ end
p1	CGGGCAGCATCAAGC	Cy3	$-(CH_2)_6-NH_2$
p2	TTTTTTTTTT	Cy3	$-(CH_2)_6-NH_2$
p3	TTTTTTTTTTTTTTT	Cy5	$-(CH_2)_6-NH_2$
p4	CGGGCAGACTCAAGC	Cy3	$-(CH_2)_6-NH_2$
p5	TTTTTTTTTTTTTTT	Cy3	$-(CH_2)_6-NH_2$
t1	GCTTGATGCTGCCCG	none	Cy5

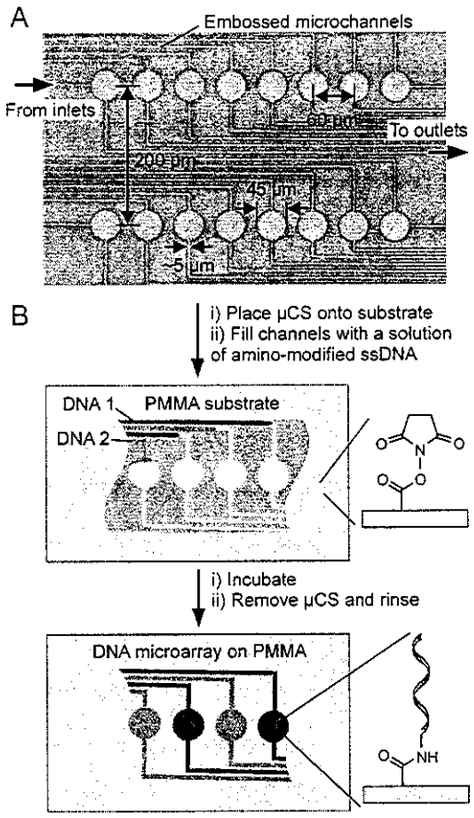

FIGURE 1. Microfluidic patterning of miniaturized DNA arrays on a plastic substrate. (A) Optical microscope image detailing the central area of a TPE-based µCS. (B) Schematic illustration of the principles governing array formation. See text for details.

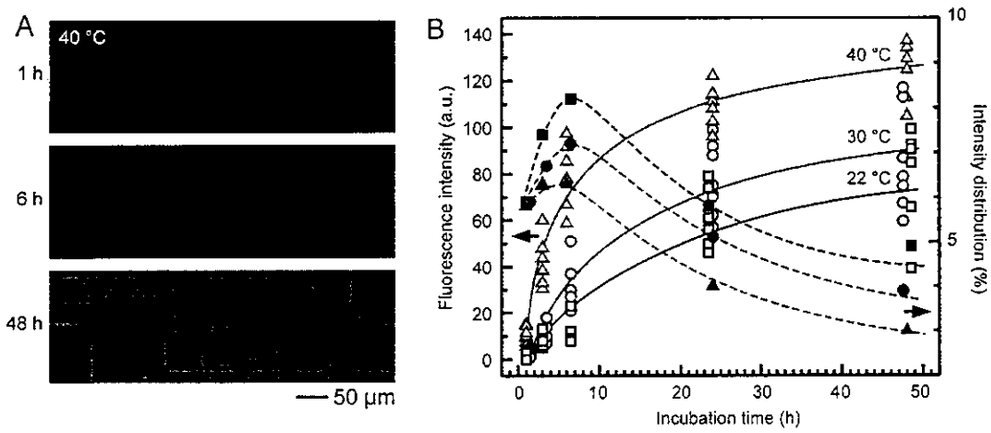

FIGURE 2. Kinetics of DNA adsorption on NHS-activated PMMA substrates as determined by fluorescence microscopy. (A) Fluorescence microscope images of rows comprising 1 × 8 spots obtained from incubation with **p1** at 40 °C for 1, 6 and 48 h. (B) Plots of fluorescence intensity (open symbols, background-corrected) and intensity distribution (filled symbols) as a function of incubation time. Here, DNA solution was incubated in a humidity chamber at 22, 30 and 40 °C (squares, circles, and triangles, respectively) for durations of between 1 and 48.5 h. The data was established by using a 32 µM solution of **p1** in PBS and a µCS with d = 4.2 µm and l ~20 mm. Lines in the graph serve as a guide to the eyes.

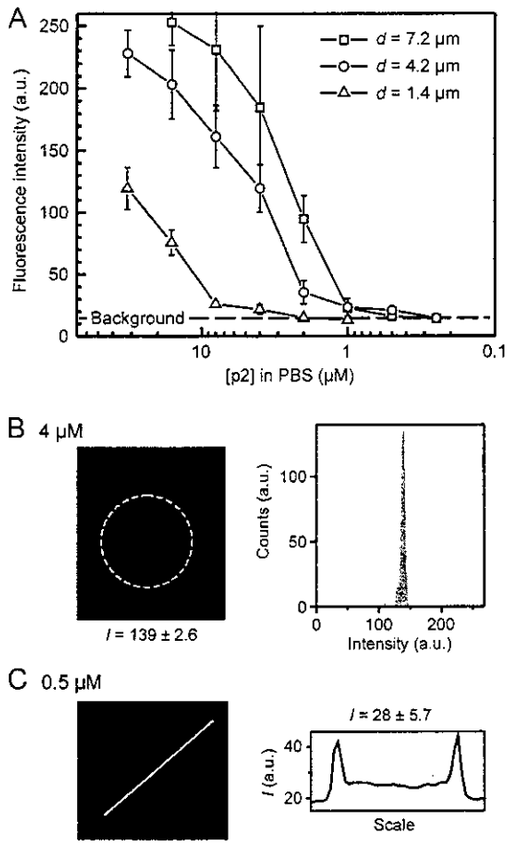

FIGURE 3. Probing the limits in DNA concentration for microfluidic spotting. (A) Plot of measured fluorescence signal as a function of **p2** concentration. The data was established using μCSs that were 7.2, 4.2, and 1.4 μm in depth (squares, circles, and triangles, respectively). Incubation was done at 22 °C for ~16 h. (B, C) Fluorescence microscope images of randomly selected spots that were obtained from 4 and 0.5 μM solutions of **p2** in PBS. Distribution of DNA within these spots is illustrated by the respective histogram and cross-sectional view. In both cases, fluidic supply channels were ~10 mm long and 4.2 μm deep.

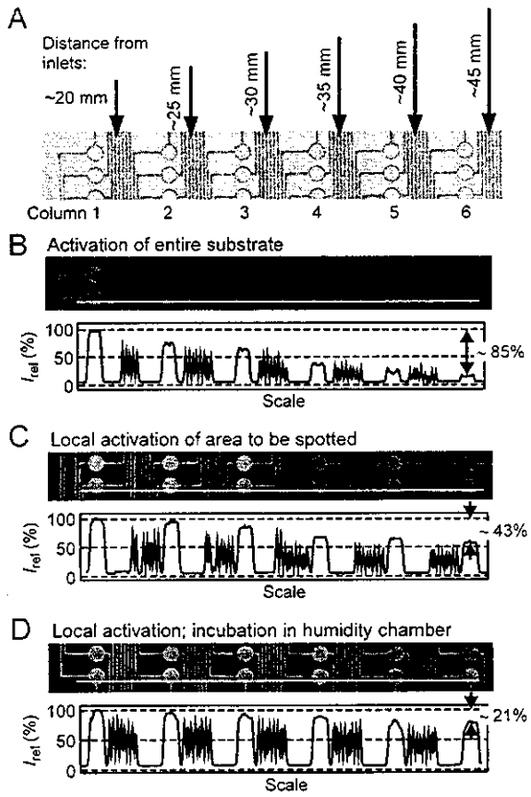

FIGURE 4. Effect of channel length on the fluorescence intensity of DNA spots. (A) Design of a μCS comprising 6 columns of spots supplied by microchannels that are 20 to 45 mm long, respectively. Each set of channels is connected to one macroscopic inlet. Outgoing channels were 15 mm long. (B–D) Fluorescence microscope images and corresponding intensity profiles detailing sections of 6 × 2 spots obtained from immobilization of **p1** with PMMA at room temperature for 16 h. (B) The measured intensity decreased considerably with the channel length due to unproductive loss of DNA molecules during transport when the entire surface of the substrate was activated with NHS and incubation was performed at ambient conditions. (C) Local activation of the substrate at the target area notably reduced the loss of DNA molecules and improved array uniformity to some extent for similar conditions of incubation. (D) Differences in intensity of spots were marginal when a locally activated substrate and a humidity-controlled incubation chamber were used.

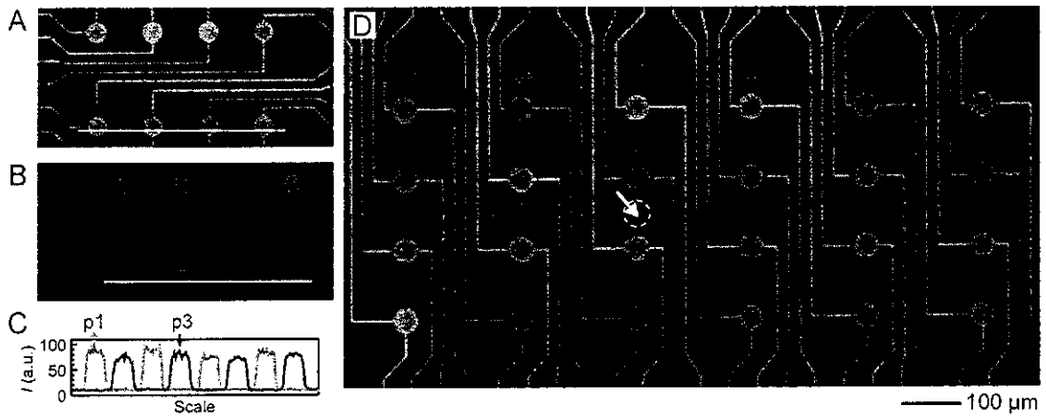

FIGURE 5. Parallel spotting of multiple probes. (A, B) Fluorescence micrographs of **p1** and **p3** as imaged in the Cy3 (green) and Cy5 channel (red), respectively. Probes were immobilized in parallel using the same µCS. (C) Intensity profiles corresponding to the locations that are indicated by the white line in each image. (D) Array of 6 × 8 spots on a Zeonor® substrate obtained by recombination of images acquired in the Cy3 and Cy5 channels. The arrow marks the only defect detectable in this array.

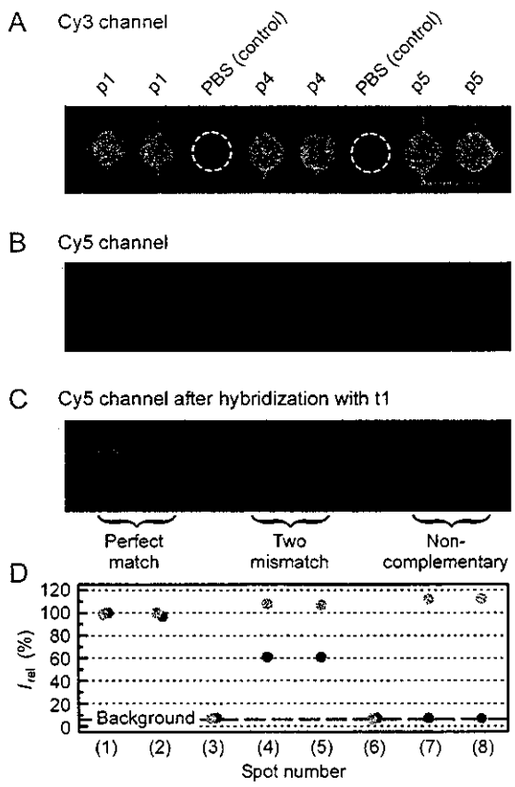

FIGURE 6. Hybridization essay comprising three DNA probes on PMMA and one target oligonucleotide. (A) Fluorescence microscope image of an array that was obtained from incubation with **p1**, **p4**, and **p5** at a concentration of 32 μM in PBS, respectively. (B) Corresponding area viewed in the Cy5 channel. (C) Hybridization pattern (Cy5 emission) after passive incubation with **t1**. (D) Plot of fluorescence intensities before and after hybridization (green and red circles, respectively). The data was normalized by defining one of the **p1** spots as to be 100%.